Practical rotation angle measurement method by monocular vision

Hongxin Dong,[1,*] Qiang Fu,[1] Xu Zhao,[1] Quan Quan,[1,2] and Ruifeng Zhang[3]

[1]School of Automation Science and Electrical Engineering, Beihang University, No. 37, XueYuan Road, HaiDian District, Beijing 100191, China

[2]State Key Laboratory of Virtual Reality Technology and Systems, Beihang University, No. 37, XueYuan Road, HaiDian District, Beijing 100191, China

[3]Beijing Aviation Engineering Technology Research Center, No. 6, Jingbei East Road, Fengtai District, Beijing 100076, China

*Corresponding author: dhx_buaa@buaa.edu.cn

Received 1 October 2014; revised 8 December 2014; accepted 8 December 2014; posted 9 December 2014 (Doc. ID 223990); published 14 January 2015

A practical vision-based method is proposed to measure single axis rotation angles. Compared with existing angle measurement methods, the proposed method is more practical because of the simple equipment required and an easy installation. Furthermore, unlike most existing methods, the proposed method does not require the rotation axis information at all. The information is calibrated by two-view geometry of the single axis motion. Then, on the basis of the calibration results, an angle estimation algorithm with point matching is proposed. Experiments on synthetic and real images show that the proposed method is robust with respect to image noises and occlusion. A measurement accuracy of less than 0.1° is obtained in real experiments only using a provided camera and a normal printed checkboard. Moreover, a single axis rotation angle measurement MATLAB toolbox is developed, which is available online (http://quanquan.buaa.edu.cn/Anglemeasurementtoolbox.html). © 2015 Optical Society of America

OCIS codes: (150.1488) Calibration; (150.1135) Algorithms; (350.4600) Optical engineering; (330.7325) Visual optics, metrology.

http://dx.doi.org/10.1364/AO.54.000425

1. Introduction

Measuring angles of a rotation device is a regular and important activity in various engineering fields. Existing rotation angle measurement methods are mainly classified into three categories: mechanical methods, electromagnetic methods, and optical methods. Mechanical methods use a multigear disk on the rotation axis to measure angles [1]. Electromagnetic methods adopt electromagnetic angle indexing technologies to obtain angles. Optical methods have a great variety, including the fiber method [2], the optical internationalization method [3], the laser interference method [4], the ring laser method [5], the vision-based angle measurement method [6,7], and so forth. These three types of methods have different characters and are suitable for different applications.

In industrial areas, it is very necessary to test and correct mounted angle measurement sensors, and sometimes this work should be done in working field. To achieve this requires measuring rotation angles with simple equipment that is easy to carry and install. Generally, it is not allowed to dismantle rotation devices for convenience, and in most situations the rotation axis is invisible or difficult to obtain accurately. For instance, aircraft maintainers are often required to test and correct angle measurement sensors of aircraft rudders, as shown in Fig. 1, without

1559-128X/15/030425-11$15.00/0

Fig. 1. Aircraft tail with elevating rudder and yaw rudder.

dismantling the rudders when working in the field. These constraints make most of the existing methods somewhat inapplicable or inconvenient. Mechanical methods require modifying the original structure of the rotation devices, while electromagnetic methods need prior calibration and complex installation. Optical methods excluding the vision-based method often rely on some special and expensive equipment such as lasers, prisms, or gratings, which are also difficult to install. These motivate us to propose a practical and convenient rotation angle measurement method.

The vision-based method is very suitable for the above situation due to its noncontact nature and briefness. However, as far as the authors know, existing vision-based methods are inapplicable when no rotation axis information is available. In [6], in order to obtain rotation angles, the proposed method is confined to the case where the camera optical axis and the rotation axis are both vertical to the reference target plane. In [7], the proposed method requires information about the image position of the intersection point of the target and the rotation axis.

A feasible way to obtain rotation axis information is to estimate it from a rotation image sequence by analyzing properties of the single axis rotation. This is a special case of the general camera motion, which is estimated by two distinct approaches including optical flow methods and feature-based methods [8]. Optical flow methods recover three-dimensional (3D) camera motions by analyzing the instantaneous changes in brightness values of the image sequence. Researchers have paid a lot of attention to estimating the camera motion from optical flow. Park *et al.* [9] proposed a novel method to estimate camera motion parameters from the linear composition of several optical flow models. In [10,11], gradient-based optical flow algorithms were improved by using perspective information. Zhang *et al.* [12] proposed a relatively accurate and robust direct method for estimating the 3D camera motion without calculating the optical flow beforehand. In [13], the normal flow of an image sequence was introduced to reduce the time consumption. Optical flow methods have been widely used in natural scenes and are very suitable for multi-rigid-body motions. However, these methods always assume small camera motions and are rather sensitive to illumination. In contrast, feature-based methods with targets are much more robust and accurate. Therefore, in order to achieve robust results with high accuracy, the single axis motion is estimated by feature-based methods. Lots of such methods [14–17] have been developed to calibrate camera motions with different kinds of targets. In the proposed method, the most commonly used camera motion estimation method in [17] is adopted with a plane target (a checkboard or a spot array). Based on the rotation axis information estimated from the camera motion, rotation angles are estimated.

Consequently, a two-step angle measurement method is proposed including the calibration of single axis motion and the rotation angle measurement. The key idea of the first step is to obtain the relative poses between the rotation axis and the camera by calibration. Then in the second step, more effort is focused on how to improve the accuracy and robustness during the measurement.

The calibration of single axis motion is achieved by using a conic model to fit the trajectory of a feature point in many mature 3D object reconstruction systems [18,19]. However, the conic fitting is extremely sensitive to noises especially in the case where the trajectory is only generated by small-angle rotations such as in aircraft rudder angle measurement. Even if 80–100 deg of an arc of a 3D trajectory is captured, its description as a curve is very unreliable for computing parameters [20]. Therefore, the single axis motion is calibrated through two-view geometry [21]. Although it is common in 3D reconstruction, as far as the authors know, few papers deal with the rotation angle measurement problem with a plane target using two-view geometry. Finally, in order to refine calibration results, the bundle adjustment is further employed.

Based on the calibration information, a robust and accurate angle measurement algorithm with point matching is proposed. Combining the calibration results, the algorithm can remove matching ambiguities caused by occlusion. Thus, the proposed method is applicable in occlusion situations. Moreover, thanks to the point detection algorithm of checkboard [22], the calibration and measurement are auto completed with satisfying speed and robustness.

The contribution of this paper is providing a practical rotation angle measurement method and a MATLAB toolbox online. It is mainly used to test and correct angle measurement sensors. The practicality lies in three aspects: (i) simple equipment, namely only a camera with fixed focal length and a plane target; (ii) no special installation and rotation axis information requirements; and (iii) robustness with respect to image noises and occlusion.

The remainder of this paper is organized as follows: Section 2 describes some preliminaries including the coordinate transformation and the nonlinear pinhole camera model. In Section 3, the two-view geometry of single axis motion is stated as a theorem. In Section 4, the calibration and angle measurement

method are presented. Simulations and real experiments are given in Section 5. Section 6 concludes the paper with a short summary.

In this paper, the following notations are used. $\mathbb{Z}_1^n$ denotes the set of positive integers less than n; $\mathbb{R}^n$ is a Euclidean space of dimension n. $|\cdot|$ denotes the absolute value of a real number. $\|\cdot\|$ denotes the Euclidean vector norm or induced matrix norm. I_n is the identity matrix of order n. $0_{n_1\times n_2}$ denotes a zero vector or a zero matrix with dimension $n_1 \times n_2$. M^{-1} denotes the inverse matrix of a square matrix M. The symbol $[\cdot]_\times:\mathbb{R}^3 \to \mathbb{R}^{3\times 3}$ is defined as

$$\begin{bmatrix} v_x \\ v_y \\ v_z \end{bmatrix}_\times = \begin{bmatrix} 0 & -v_z & v_y \\ v_z & 0 & -v_x \\ -v_y & v_x & 0 \end{bmatrix}. \tag{1}$$

The cross product of two vectors v_1, $v_2 \in \mathbb{R}^3$ is denoted as $v_1 \times v_2 = [v_1]_\times v_2$. The element of a matrix S at the ith row and jth column is denoted as S_{ij}. The symbol vec(S) is the column vector obtained by stacking the second column of S under the first, and then the third, and so on.

2. Preliminaries

In this section, preliminaries of the proposed vision-based measurement method are introduced, including the coordinate transformation and the nonlinear camera model.

A. Coordinate Transformation

The rigid transformation between different coordinate systems is expressed by a rotation matrix and a translation vector. In this paper, the rotation matrix and translation vector from O_b-$x_by_bz_b$ to O_a-$x_ay_az_a$ are denoted as R_{ab} and T_{ab}, and $[R_{ab}, T_{ab}]$ is called the transformation matrix of the two coordinate systems.

Theorem 1. The rotation matrix and the translation vector have the following properties: (i) T_{ab} is the coordinate of O_b in O_a-$X_aY_aZ_a$; (ii) $R_{ba} = R_{ab}^T$, $T_{ba} = -R_{ba}T_{ab}$; and (iii) for three coordinate systems O_a-$X_aY_aZ_a$, O_b-$X_bY_bZ_b$, and O_c-$X_cY_cZ_c$, the relation among their rotation matrices and translation vectors is

$$R_{bc} = R_{ba}R_{ac}, \qquad T_{bc} = R_{ba}(T_{ac} - T_{ab}). \tag{2}$$

B. Nonlinear Camera Model

A linear pinhole camera model performs the transformation from P in O_w-$X_wY_wZ_w$ to the camera coordinate system O_c-$X_cY_cZ_c$, then to the image points p in O_i-X_iY_i, as shown in Fig. 2. The relation between a world point $(x_w, y_w, z_w)^T$ and its corresponding normal image point $(x_n, y_n)^T$ is written as

$$\lambda \begin{bmatrix} x_n \\ y_n \\ 1 \end{bmatrix} = [R_{cw}, T_{cw}] \begin{bmatrix} x_w \\ y_w \\ z_w \\ 1 \end{bmatrix}, \tag{3}$$

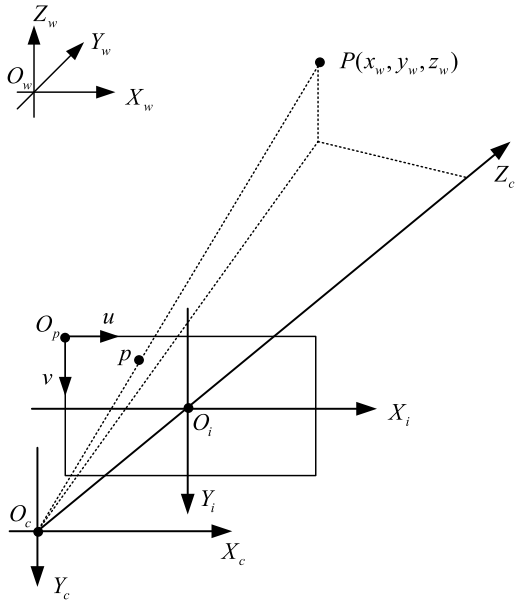

Fig. 2. Linear pinhole camera model. Four coordinate systems are involved: (i) the world coordinate system O_w-$X_wY_wZ_w$; (ii) the camera coordinate system O_c-$X_cY_cZ_c$; (iii) the image coordinate system O_i-X_iY_i; and (iv) the pixel coordinate system O_p-uv. The coordinate of O_i is (u_0, v_0) in O_p-uv.

where λ is a scale factor and $[R_{cw}, T_{cw}]$ is the transformation matrix from O_w-$X_wY_wZ_w$ to O_c-$X_cY_cZ_c$.

In fact, the camera model does not strictly satisfy the pinhole imaging model. There exist radial and tangential distortions. For higher accuracy, a widely used distortion model [17] is adopted in this paper. In order to compensate for the deviation, the real normalized image point $(x_n', y_n')^T$ is approximately obtained from $(x_n, y_n)^T$ by the following formulas:

$$\begin{cases} x_n' = \kappa x_n + 2k_3x_ny_n + k_4(r^2 + 2x_n^2) \\ y_n' = \kappa y_n + 2k_3x_ny_n + k_4(r^2 + 2y_n^2) \end{cases}, \tag{4}$$

where $\kappa = 1 + k_1r^2 + k_2r^4 + k_5r^6$, $r^2 = x_n^2 + y_n^2$, and k_1, k_2, k_3, k_4, k_5 are distortion parameters. Then, the real image point $(u, v)^T$ is obtained from

$$\begin{bmatrix} u \\ v \\ 1 \end{bmatrix} = K \begin{bmatrix} x_n' \\ y_n' \\ 1 \end{bmatrix}, \tag{5}$$

and

$$K = \begin{bmatrix} \alpha_x & 0 & u_0 \\ 0 & \alpha_y & v_0 \\ 0 & 0 & 1 \end{bmatrix}, \tag{6}$$

where α_x and α_y are the scale factors in image u and v axes; $(u_0, v_0)^T$ are the coordinates of the principal point.

For convenience of description, the image point is written as functions of involved parameters:

$$\begin{cases} u = f_u(p_{\text{in}}, R_{cw}, T_{cw}, x_w, y_w, z_w) \\ v = f_v(p_{\text{in}}, R_{cw}, T_{cw}, x_w, y_w, z_w) \end{cases}, \tag{7}$$

where the intrinsic parameter vector $p_{\text{in}} = (\alpha_x, \alpha_y, u_0, v_0, k_1, k_2, k_3, k_4, k_5)^T$.

3. Two-View Geometry of Single Axis Motion

A single axis motion consists of a set of relative motions between the scene and the camera, which is described by rotations around a single axis. There are many cases of this motion commonly occurring in computer vision applications. The most common, and the one that is used here, is the case of a static camera viewing an object rotating around a single axis. The two-view geometry of this case describes the specific geometry relations of the camera, the scene, and the single axis in two camera views. This geometry is stated as the following theorem.

Theorem 2. As shown in Fig. 3, the origin point O_a of O_a-$X_aY_aZ_a$ is on the X_c axis of O_c-$X_cY_cZ_c$, and O_b-$X_bY_bZ_b$ is obtained by rotating O_a-$X_aY_aZ_a$ around the Z_c axis by a rotation angle $\theta(\theta \neq 0)$. If the coordinate of O_a in O_c-$X_cY_cZ_c$ is $(t, 0, 0)^T$, then

$$\frac{1}{t \sin\theta} E = -[r_2]_\times + \tan\frac{\theta}{2}(r_2 r_3^T + r_3 r_2^T), \tag{8}$$

where $E = [T_{ba}]_\times R_{ba}$ and $R_{ac} = [r_1, r_2, r_3]$, $r_1, r_2, r_3 \in \mathbb{R}^3$.

Proof. See Appendix A.

Next it will be seen that R_{ac}, t and θ are determined uniquely by E. Since $[r_2]_\times^T = -[r_2]_\times$, it follows that

$$\frac{1}{t \sin\theta}(E^T - E) = 2[r_2]_\times.$$

Furthermore, since $\|r_2\| = 1$, then

$$r_2 = \frac{v_s}{\|v_s\|}, \tag{9}$$

$$\mu = t \sin\theta = \frac{\|v_s\|}{2}, \tag{10}$$

where $v_s = (S_{3,2}, S_{1,3}, S_{2,1})^T$ and $S = E^T - E$. From Eq. (8), the following equation holds:

$$\left(\frac{1}{\mu}E + [r_2]_\times\right) r_1 = \tan\frac{\theta}{2}(r_2 r_3^T + r_3 r_2^T) r_1.$$

Consequently, $(\frac{1}{\mu}E + [r_2]_\times) r_1 = 0$ for $r_3^T r_1 = 0$ and $r_2^T r_1 = 0$. This implies that r_1 is the solution of

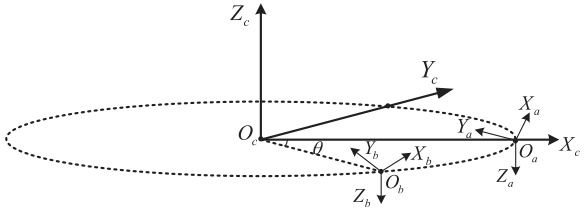

Fig. 3. Two-view geometry of single axis motion.

$$\left(\frac{1}{\mu}E + [r_2]_\times\right) x = 0, \quad \text{subject to } \|x\| = 1, \tag{11}$$

which is the unit singular vector of $\frac{1}{\mu}E + [r_2]_\times$ corresponding to the smallest singular value. With r_1, r_2 in hand, $R_{ac} = [r_1, r_2, r_1 \times r_2]$ is obtained. Let us revisit Eq. (8). The rotation angle θ is obtained as

$$\theta = 2 \arctan\left(\frac{A^T B}{A^T A}\right), \tag{12}$$

where $A = \text{vec}(r_2 r_3^T + r_3 r_2^T)$ and $B = \text{vec}(\frac{1}{\mu}E + [r_2]_\times)$. Finally, since θ is not zero, t is determined by

$$t = \frac{\mu}{\sin\theta}. \tag{13}$$

The aforementioned description is summarized as the following theorem.

Theorem 3. Suppose that the conditions of Result 1 hold and $R_{ac} = [r_1, r_2, r_1 \times r_2]$. Then, r_1, r_2, t and θ in Eq. (8) are obtained according to Eqs. (9), (11), (13), and (12), respectively.

4. Process of Angle Measurement

In this section, a practical method to measure rotation angles is proposed. First, the angle measurement problem is formulated in Section 4.A. Then two steps of the proposed method are presented in Sections 4.B and 4.C. In the first step, required information including camera intrinsic parameters and relative pose information is calibrated from a rotation image sequence. In the second step, based on the calibration results, an angle estimation algorithm with point matching is proposed to remove the matching ambiguity caused by occlusion. Figure 4 describes the process of angle measurement.

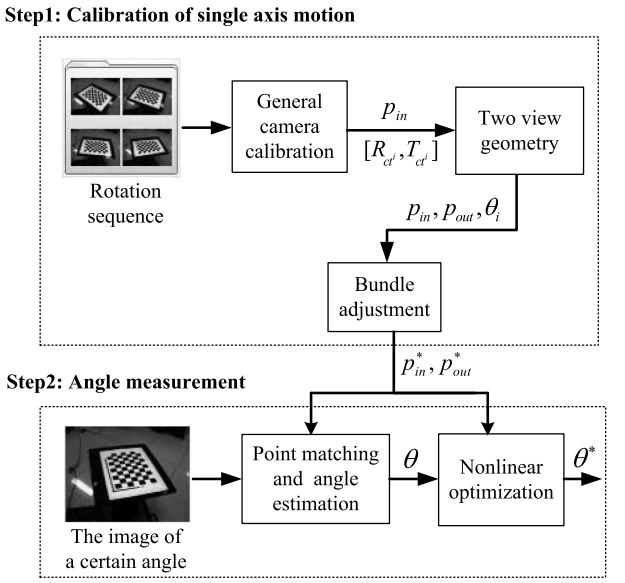

Fig. 4. Process of the proposed rotation angle measurement method. Details of step 1 and step 2 are described in Sections 4.B and 4.C, respectively.

A. Problem Formulation

The world coordinate system is established as in Fig. 5, where the rotation axis is aligned with the Z_w axis. The reference target coordinate system is denoted as O_t-$X_tY_tZ_t$ with the world coordinate of its origin point O_t being $T_{wt} = (t, 0, 0)^T$, $t > 0$. All target points are in the $X_tO_tY_t$ plane, that is, the target coordinates of all these points are in the form of $(x_t, y_t, 0)^T$. Furthermore, if $(x_w(\theta), y_w(\theta), z_w(\theta))^T$ is the world coordinate of a target point $(x_t, y_t, 0)^T$ with respect to a rotation angle θ, then it has the following form:

$$\begin{bmatrix} x_w(\theta) \\ y_w(\theta) \\ z_w(\theta) \end{bmatrix} = \begin{bmatrix} \cos\theta & -\sin\theta & 0 \\ \sin\theta & \cos\theta & 0 \\ 0 & 0 & 1 \end{bmatrix} \left(R_{wt} \begin{bmatrix} x_t \\ y_t \\ 0 \end{bmatrix} + T_{wt} \right),$$

Let $[R_{cw}, T_{cw}]$ denote the transformation matrix from O_w-$X_wY_wZ_w$ to the camera coordinate system O_c-$X_cY_cZ_c$. Then, according to Eqs. (7), the image point is written as

$$\begin{aligned} u &\triangleq g_u(p_{\text{in}}, p_{\text{out}}, \theta, x_t, y_t) \\ &= f_u(p_{\text{in}}, R_{cw}, T_{cw}, x_w(\theta), y_w(\theta), z_w(\theta)), \end{aligned} \tag{14}$$

$$\begin{aligned} v &\triangleq g_v(p_{\text{in}}, p_{\text{out}}, \theta, x_t, y_t) \\ &= f_v(p_{\text{in}}, R_{cw}, T_{cw}, x_w(\theta), y_w(\theta), z_w(\theta)). \end{aligned} \tag{15}$$

Here, the extrinsic parameter vector $p_{\text{out}} \in \mathbb{R}^{10}$ has the following form:

$$p_{\text{out}} = ((v_{\text{rot}}^{wt})^T, (v_{\text{rot}}^{cw})^T, t, T_{cw}^T)^T,$$

where $v_{\text{rot}}^{wt} \in \mathbb{R}^3$ and $v_{\text{rot}}^{cw} \in \mathbb{R}^3$ are Rodrigues's vectors [23] corresponding to R_{wt} and R_{cw}.

The calibration of single axis motion in Section 4.B aims to obtain the estimation of p_{in} and p_{out} from a rotation image sequence, while the second step in Section 4.C estimates the rotation angle θ of a certain image.

B. Calibration of Single Axis Motion

In this section, a method based on two-view geometry is proposed to estimate p_{in} and p_{out} from a rotation image sequence. The image sequence consists of a reference image and m images taken with respect to different rotation angles $\theta_i, i = 1, \cdots, m$. In order to correspond detected interesting points and target points easily, all interesting points in the image sequence should be detected out; that is, these images for calibration must be taken without occlusion.

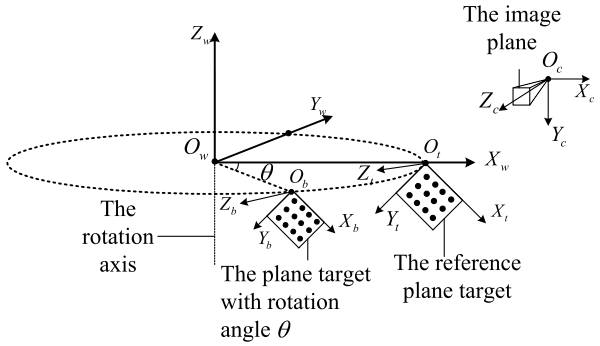

Fig. 5. Projection model of the single axis motion. The rotation axis is aligned with the Z_w axis. O_b-$X_bY_bZ_b$ is obtained by rotating the reference target coordinate system O_t-$X_tY_tZ_t$ by θ.

The calibration of single axis motion is a special case of general camera calibration, on which many algorithms have been proposed [14–17]. Carrying out a general camera calibration on the image sequence, we obtain the intrinsic parameter vector p_{in} and extrinsic parameters of the image sequence, denoted as $[R_{ct^i}, T_{ct^i}]$, $i = 0, 1, \cdots, m$, respectively. Here $[R_{ct^0}, T_{ct^0}]$ is the transformation matrix from the reference target coordinate system O_t-$X_tY_tZ_t$ to O_c-$X_cY_cZ_c$, and $[R_{ct^i}, T_{ct^i}]$ is the transformation matrix from the target coordinate system with respect to rotation angle θ_i to O_c-$X_cY_cZ_c$. Based on this information and the two-view geometry of single axis motion, extrinsic parameters including p_{out} and rotation angles $\theta_1, \cdots, \theta_m$ are estimated. The details are given as follows.

1. *Extrinsic Parameters Estimation*

According to Theorem 1 (ii) and (iii), the transformation matrix $[R_{t^it^0}, T_{t^it^0}]$ from the ith target to the reference target is calculated by

$$R_{t^it^0} = R_{ct^i}^T R_{ct^0} \quad \text{and} \quad T_{t^it^0} = R_{ct^i}^T (T_{ct^0} - T_{ct^i}). \tag{16}$$

With $R_{t^it^0}$ and $T_{t^it^0}$, R_{cw}, t and θ_i are obtained by Theorem 3. Furthermore, once R_{cw} and t are determined, $[R_{wt}, T_{wt}]$ is obtained from

$$R_{wt} = R_{cw}^T R_{ct^0} \quad \text{and} \quad T_{wt} = R_{cw}^T T_{ct^0} + (t, 0, 0)^T. \tag{17}$$

2. *Bundle Adjustment*

Parameters $p_{\text{out}}, \theta_1, \cdots, \theta_m$ calculated above are refined through the bundle adjustment, which gains the maximum likelihood estimation of involved parameters [24]. The optimal estimation of p_{in}, $p_{\text{out}}, \theta_i, i = 1, 2, \cdots, m$ is obtained by nonlinear minimization of the sum of the squared distance between reprojection points and detected corners. According to Eqs. (14) and (15), for the i th target, the reprojection point $(u_i^j, v_i^j)^T$ corresponding to the jth out of n plane target points $(x_t^j, y_t^j)^T$ is written as

$$\begin{cases} u_i^j = g_u(p_{\text{in}}, p_{\text{out}}, \theta_i, x_t^j, y_t^j) \\ v_i^j = g_v(p_{\text{in}}, p_{\text{out}}, \theta_i, x_t^j, y_t^j) \end{cases}.$$

Thus, the optimization problem is formulated as

$$(p_{\text{in}}^*, p_{out}^*, \theta_1^*, \cdots, \theta_m^*) = \arg \min_{p_{\text{in}}, p_{\text{out}}, \theta_1, \cdots, \theta_m} \sum_{i=0}^{m} \sum_{j=1}^{n} E_r^{i,j},$$

where $E_r^{i,j} = (\bar{u}_i^j - u_i^j)^2 + (\bar{v}_i^j - v_i^j)^2$ and $(\bar{u}_i^j, \bar{v}_i^j)^T$ is the coordinate of the detected corner corresponding to $(u_i^j, v_i^j)^T$. The nonlinear optimization can be solved by the Levenberg–Marquardt algorithm [25].

C. Rotation Angle Measurement

In this section, the camera takes an image of the plane target rotating to a certain position. Unlike the first step, the plane target can be occluded partly. An angle estimation algorithm with point matching is proposed. This algorithm consists of four steps: possible matching selection, histogram voting, one-to-one point matching, and nonlinear optimization. The realization of this algorithm is shown as in Algorithm 1.

Algorithm 1 Point Matching and Angle Estimation

Input: Calibration results p_{in}^*, R_{cw}, t, R_{wt}, T_{wt}, target points $(x_t^i, y_t^i), i = 1, 2, \cdots, n^{***}$,
detected interesting points $(\bar{u}_c^j, \bar{v}_c^j), j = 1, 2, \cdots, N_c$, the grid length d.
Output: Rotation angle θ^*.
Initialize: $\tau_m = 0.1d$, $\tau_\alpha = 1°$, $H_k = 0$, $k = 1, \cdots, 361$.

```
For i = 1 to n
  For j = 1 to N_c
    Calculate T_{i,j} = Sc(ū_c^j, v̄_c^j, x_t^i, y_t^i);
    If T_{i,j} ≤ τ_m
      Calculate θ_{i,j};
      For k = 1 to 361
        If k ∈ (θ_{i,j} − τ_α + 181°, θ_{i,j} + τ_α + 181°)
          H_k = H_k + 1.
        end
      end
    end
  end
end
θ = (arg max_k{H_k} − 181)°.
For j = 1 to N_c
  M_j = arg min_l T_{l,j}, satisfy θ_{i,j} ∈ (θ − τ_α, θ + τ_α) and T_{l,j} ≤ τ_m.
end
Nonlinear optimization to refine θ.
```

1. Possible Matching Selection

Suppose that N_c interesting points are detected and denoted as $(\bar{u}_c^j, \bar{v}_c^j)^T, j = 1, 2, \cdots, N_c$. Here $0 < N_c \le n$. The purpose of this section is to find all possible matching point pairs in

$$\Omega = \{(\bar{u}_c^j, \bar{v}_c^j)^T \leftrightarrow (x_t^i, y_t^i)^T | j \in \mathbb{Z}_1^{N_c}, i \in \mathbb{Z}_1^n\}.$$

The trajectory of a target point is a circle at a plane parallel to $z_w = 0$. This property is used to judge whether an interesting point $(u, v)^T$ and a target point $(x_t, y_t, 0)^T$ are matched. Concretely, if $(u, v)^T$ and $(x_t, y_t, 0)^T$ are matched, then the following equation holds:

$$\bar{x}_w^2 + \bar{y}_w^2 = x_w^2 + y_w^2, \qquad z_w = \bar{z}_w, \tag{18}$$

where $(x_w, y_w, z_w)^T$ is the world coordinate of $(x_t, y_t, 0)^T$, and $(\bar{x}_w, \bar{y}_w, \bar{z}_w)^T$ is the world coordinate corresponding to $(u, v)^T$. Since R_{cw}, t, R_{wt}, T_{wt} are already calibrated, $(x_w, y_w, z_w)^T$ is obtained from

$$\begin{bmatrix} x_w \\ y_w \\ z_w \end{bmatrix} = R_{wt} \begin{bmatrix} x_t \\ y_t \\ 0 \end{bmatrix} + T_{wt},$$

and $(\bar{x}_w, \bar{y}_w, \bar{z}_w)^T$ is computed from

$$\bar{x}_w = \rho r_n^T r_1 + t, \bar{y}_w = \rho r_n^T r_2, \bar{z}_w = z_w,$$

where $r_n = (x_n, y_n, 1)^T$, $\rho = \frac{z_w}{r_n^T r_3}$, $R_{cw} = [r_1, r_2, r_3]$, and $(x_n, y_n)^T$ is the normalized projection point of $(u, v)^T$. Here, $(x_n, y_n)^T$ is obtained by solving Eqs. (4) after $(x_n', y_n')^T$ is calculated by

$$\begin{bmatrix} x_n' \\ y_n' \\ 1 \end{bmatrix} = K^{-1} \begin{bmatrix} u \\ v \\ 1 \end{bmatrix}.$$

Therefore, for $(u, v)^T \leftrightarrow (x_t, y_t)^T$, a computable matching score may be given as

$$Sc(u, v, x_t, y_t) = \sqrt{\bar{x}_w^2 + \bar{y}_w^2} - \sqrt{x_w^2 + y_w^2}. \tag{19}$$

This score implies that a possible correct matching deserves a zero score. In consideration of noises, a threshold τ_m is selected, which means if $Sc(u, v, x_t, y_t) \le \tau_m$, then $(u, v)^T$ and $(x_t, y_t, 0)^T$ are said to be possibly matched. One can set $\tau_m = 0.1d$; here d is the minimum length of different target points. The set of possible matching point pairs with respect to this score is written as

$$\Omega_0 = \{(\bar{u}_c^j, \bar{v}_c^j)^T \leftrightarrow (x_t^i, y_t^i)^T | Sc(\bar{u}_c^j, \bar{v}_c^j, x_t^i, y_t^i) \le \tau_m\}.$$

Generally, not all elements in Ω_0 are correctly matched. Image noises may introduce wrong matchings to it. Moreover, in some cases, such as the case where two different target points have the same Z_w components, wrong matchings definitely exist. These wrong matchings could be removed by analyzing the distribution of possible rotation angles.

2. Histogram Voting

For every $(\bar{u}_c^j, \bar{v}_c^j)^T \leftrightarrow (x_t^i, y_t^i)^T$ in Ω_0, the rotation angle $\theta_{i,j}$ is calculated by

$$\begin{bmatrix} \bar{x}_w^j \\ \bar{y}_w^j \\ \bar{z}_w^j \end{bmatrix} = \begin{bmatrix} \cos\theta_{i,j} & -\sin\theta_{i,j} & 0 \\ \sin\theta_{i,j} & \cos\theta_{i,j} & 0 \\ 0 & 0 & 1 \end{bmatrix} \begin{bmatrix} x_w^i \\ y_w^i \\ z_w^i \end{bmatrix}, \tag{20}$$

where (x_w^i, y_w^i, z_w^i) are the world coordinates of $(x_t^i, y_t^i, 0)^T$ and $(\bar{x}_w^j, \bar{y}_w^j, \bar{z}_w^j)^T$ are the world coordinates corresponding to $(\bar{u}_c^j, \bar{v}_c^j)^T$. Let Θ denotes the set of rotation angles corresponding to elements in Ω_0:

$$\Theta = \{\theta_{i,j} \in (-180°, 180°) | (\bar{u}_c^j, \bar{v}_c^j)^T \leftrightarrow (x_t^i, y_t^i)^T \in \Omega_0\}.$$

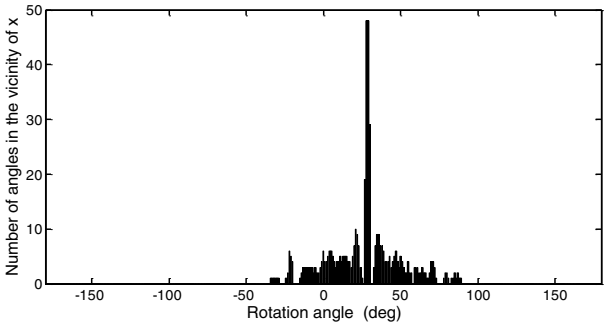

Fig. 6. Sample histogram H from synthetic data. The rotation angle of this example is 30°.

Generally, most elements of Θ are distributed in the vicinity of the real rotation angle if sufficient interesting points are detected. Thus, the rotation angle θ may be estimated roughly by analyzing the distribution of Θ. In detail, a histogram H with 361 bins is built, where the k th bin H_k contains the number of elements in $\Theta \cap [(k-181)^\circ - \tau_\alpha, (k-181)^\circ + \tau_\alpha]$. Here, τ_α is a threshold for describing the distribution interval of angles corresponding to correct matchings, and a suitable value of it is 1°, just as we have done in our experiment part. A sample histogram H is shown in Fig. 6. If the calibration results are well estimated, the histogram has a very narrow peak at the correct rotation angle θ, that is,

$$\theta = (\arg\max_k\{H_k\} - 181)^\circ. \tag{21}$$

The estimate θ in Eq. (21) has given a rough rotation angle. For higher accuracy, the following matching and nonlinear optimization are required.

3. *One-to-One Point Matching*

In Ω_0, an interesting point may match with several target points. Combining the information of rotation angle θ, the one-to-one point matching M_j of $(\bar{u}_c^j, \bar{v}_c^j)^T$ is defined as

$$M_j = \arg\min_i Sc(\bar{u}_c^j, \bar{v}_c^j, x_t^i, y_t^i), \text{subject to}$$
$$\theta_{i,j} \in (\theta - \tau_\alpha, \theta + \tau_\alpha) \quad \text{and} \quad T_{l,j} \le \tau_m.$$

If no target point satisfies the constraint, then $M_j = 0$, which happens when wrong corners are detected.

4. *Nonlinear Optimization*

A nonlinear minimization of the sum of the squared distance between reprojection points $(u^{M_j}, v^{M_j})^T$ and the corresponding detected corners $(\bar{u}_c^j, \bar{v}_c^j)^T$ is carried out to refine the rotation angle. The optimization problem is formulated as

$$\theta^* = \arg\min_\theta \sum_{j=1}^{N_c} \delta_j[(\bar{u}_c^j - u^{M_j})^2 + (\bar{v}_c^j - v^{M_j})^2],$$

where $\delta_j = \begin{cases} 1, & \text{if } M_j > 0, \\ 0, & \text{others,} \end{cases}$ It can be solved by the Levenberg–Marquardt algorithm [25].

5. Experiments

The proposed method is tested on both synthetic data and real images with the checkboard [16], a specific plane target widely used in camera calibration. First, synthetic data is generated to evaluate the measurement error of the proposed method in Section 5.A. Then, in Section 5.B, real experiments with a printed checkboard and a Basler camera are carried out on a turntable to demonstrate the correctness of the proposed method.

A. Synthetic Data

The simulation is carried out with a virtual camera, whose image size is 640 pixels × 480 pixels. The internal parameters of the camera are

$$\alpha_x = 800 \text{ pixels}, \quad \alpha_y = 800 \text{ pixels}$$
$$u_0 = 322 \text{ pixels}, \quad v_0 = 243 \text{ pixels}$$
$$k_1 = 0, \quad k_2 = 0, \cdots, k_5 = 0.$$

A checkboard with size of 6 × 8 and grid length $d = 30$ mm is chosen as the plane target. The relative poses of the reference checkboard, the rotation axis, and the camera are set as

$$v_{\text{rot}}^{wt} = (-0.2917, 0.4050, -0.2588)^T,$$
$$v_{\text{rot}}^{cw} = (-2.2163, 1.0434, -0.0574)^T,$$
$$t = 200 \text{ mm}, \quad T_{cw} = (30, 540, -440)^T \text{ mm}.$$

Two thresholds are set as $\tau_m = 0.1d = 3$ mm, $\tau_\alpha = 1^\circ$ through the whole simulation. As described in Section 4.B, the calibration image sequence requires being taken without occlusion, which occurs when the target is rotating in the range of (0°,90°) in the simulation experimental setting. Suppose that m angles are randomly chosen in the interval (0°,90°) to generate the image sequence for calibration. Gaussian noises with zero mean and a standard deviation of σ are added to projected image points.

The angle measurement error e(deg) is measured by the maximum absolute value of rotation angle errors. Concretely, 100 test angles uniformly distributed in (0°,90°) are chosen. Suppose that real test angles and those estimated by the proposed method are denoted as $\beta_1^*, \beta_2^*, \cdots, \beta_{100}^*$ and $\beta_1, \beta_2, \cdots, \beta_{100}$, respectively; then e is defined as

$$e = \max_{i=1}^{100}(|\beta_i^* - \beta_i|). \tag{22}$$

The angle measurement error is mainly affected by two factors: the number of calibration images m and noise level σ. To measure their effects, for a certain (m, σ), 100 tests are carried out. The angle measurement error with respect to (m, σ) is represented by the mean μ_e and variance Σ_e of measurement errors obtained by these 100 tests, which are calculated by

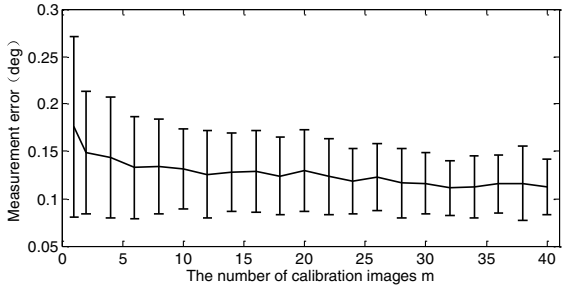

Fig. 7. Measurement errors for different m.

$$\mu_e = \frac{1}{100}\sum_{i=1}^{100} e_i, \qquad \Sigma_e = \frac{1}{99}\sum_{i=1}^{100}(e_i - \mu_e)^2, \tag{23}$$

where e_i is the angle measurement error of the ith test. Figure 7 shows the error bar of measurement errors varying with $m(1, 2, 4, 6, 8, \cdots, 40)$ when $\sigma = 1$. As shown in the figure, the measurement error decreases with the increase of m, and when $m \geq 10$, the reduction rate becomes rather small. Thus in the following tests, m is set to be 10 to reduce time consumption under the premise of ensuring accuracy. Figure 8 shows the error bar of measurement errors varying with $\sigma(0, 0.2, 0.4, \cdots, 4)$ when $m = 10$. The angle errors increase almost linearly with the increase of the noise level. Even when $\sigma = 4$, a typical large noise in practice, the proposed method can gain correct results, which demonstrates its robustness against noises.

To show the effectiveness of the proposed method in precision angle measurement, the proposed method is tested on synthetic data with $\sigma = 0, 0.01, 0.02, \cdots, 0.1$ and $m = 10$. In reality, these noise levels are reachable [6]. The result is shown in Fig. 9, which demonstrates the high accuracy with low noise levels of the proposed method.

B. Real Images

Our real experiments are implemented on a controlled mechanical turntable provided by [26] with a Basler scA640-120gm/gc camera and a printed target. A MATLAB angle measurement toolbox is developed and is available online [27]. The turntable has a measurement precision of 0.01°, a minimum rotation angle of 0.09°, and a measurement range of $(-144°, 144°)$. The resolution of the camera is

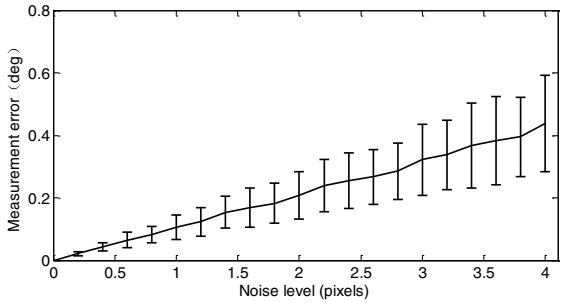

Fig. 8. Measurement errors for different noise levels.

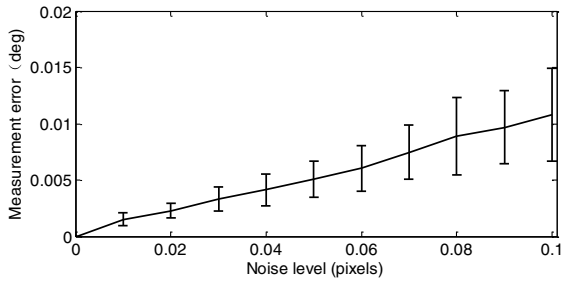

Fig. 9. Measurement errors for different small noise levels.

658 pixels × 492 pixels, and the effective focal length is about 800 pixels. The plane target we used is a checkboard with size 6×9 and grid length $d = 30$ mm. Two thresholds τ_m and τ_α are set as 3 mm and 1°, respectively, in real experiments, and interesting points are detected by Andreas's method [22]. Two different installations, as shown in Fig. 10, are tested in real experiments.

1. *Measurement Range*

The theoretical angle measurement range is determined by whether interesting points could be extracted from images with respect to angles in the interval. It changes with respect to the relative poses of the camera, the plane target, and the rotation axis. The theoretical ranges of Installation 1 and Installation 2 are $(-90°, 90°)$ and $(-180°, 180°)$, respectively. However, for Installation 1, the corner detection would introduce very large noises in some special camera views, such as shown in Fig. 11. To avoid this, it is necessary to define a measurement range of a certain installation. Let $d_{\max}$ and $d_{\min}$ denote the

(a) Installation 1

(b) Installation 2

Fig. 10. Two different installations of the camera, the plane target, and the rotation axis. (a) Installation 1 with measurement range of $(-54°, 54°)$ and (b) Installation 2 with measurement range of $(-180°, 180°)$

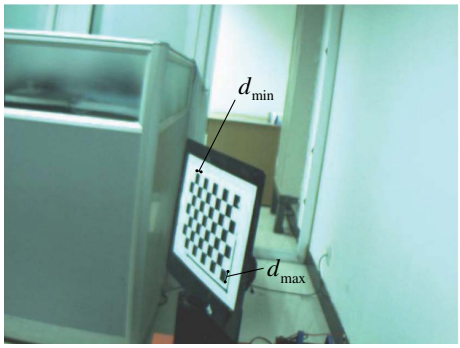

Fig. 11. Sample of bad situations. $d_{\max}$ denotes the longest grid of the image while $d_{\min}$ denotes the shortest one.

longest and the shortest grid in an image, respectively, as shown in Fig. 11. $d_{\max}$ and $d_{\min}$ can be calculated by pixel coordinates of interesting points. If $d_{\max} > 1.5d_{\min}$, then the image is not eligible. According to the principle, a judgement is carried out in the proposed method before interesting points of an image are used. One can roughly judge whether the installation is suitable by testing if images with respect to the smallest and largest angles are eligible. According to the above principle, the measurement range of Installation 1 is roughly set as $(-54°, 54°)$ and that of Installation 2 is set as $(-180°, 180°)$.

2. *Measurement Accuracy*

To obtain the measurement accuracy of the proposed method, measured rotation angles are compared with rotation angles given by the turntable. The angle errors e is written as

$$e = \alpha_t - \alpha_p, \tag{24}$$

where α_t is the angle given by the turntable, and α_p is the corresponding calculated angle. Angle errors of the two installations are shown in Fig. 12. Since the measurement range of the turntable is $(-144°, 144°)$, only angles in the interval are measured for Installation 2. As shown, the angle errors of both installation are pretty close to the angles given by the turntable. A measurement accuracy of less than 0.1° is achieved using simple devices.

3. *Execution Time*

The computational performance is evaluated on MATLAB 2012 on a personal computer with Intel Xeon W3550 processor at 3.07 GHz. The execution times of calibration, corner detection, and angle estimation are measured separately for both installations. Results are shown in Table 1. The execution times of calibration for both installations are measured when $m = 16$. For Installation 1, the execution time is the mean time of 61 images without occlusion in the range $(-54°, 54°)$, while for Installation 2, the execution time is the mean time of 160 images without occlusion in the range $(-144°, 144°)$. As shown in Table 1, the performance is acceptable for the purpose of testing and correcting angle measurement sensors in the working field. Moreover, if the code is programmed in C, the computational time can be greatly reduced.

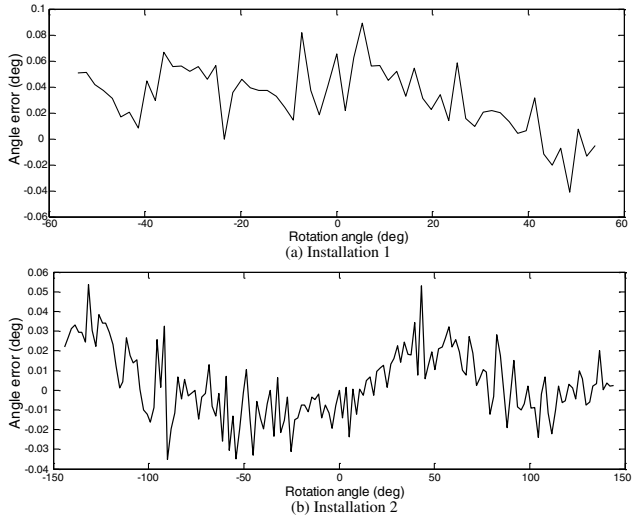

Fig. 12. Angle errors of two different installations. (a) Angle errors of 61 images without occlusion in the range $(-54°, 54°)$ for Installation 1; (b) angle errors of 160 images without occlusion in the range $(-144°, 144°)$ for Installation 2.

Table 1. Estimation Runtime

	Step 1	Step 2	
	Calibration (s)	Corner Detection (s)	Angle Estimation (s)
Installation 1	40.85	0.7188	0.0642
Installation 2	30.98	0.5654	0.0659

4. *Measurement Resolution*

The minimum resolution angle is the smallest angle which could be perceived by the proposed method in theory. It is related to the camera resolution, the relative poses of the camera with respect to the plane target, and the accuracy of corner detection, which makes it difficult to obtain an accurate value of the minimum resolution. Therefore, instead of determining the theoretical resolution value, we estimate it by comparing with the turntable. For Installation 2, we measure the minimum rotation angles of the turntable using the proposed method. Results are shown in Table 2. As shown, the proposed method is able to realize tiny angles; specifically, the

Table 2. Angle Errors of Small Angles for Installation 2

α_t(deg)	e(deg)	α_t(deg)	e(deg)
0.09	0.008	45.09	−0.019
0.18	0.017	45.18	−0.001
0.27	0.011	45.27	0.004
0.36	0.007	45.36	0.003
0.45	0.002	45.45	−0.006

Table 3. Angle Errors with Occlusion for Installation 2

α_t(deg)	e(deg)	α_t(deg)	e(deg)
29.85	0.034	93.76	−0.002
55.72	0.006	−42.88	0.063
78.34	0.010	−68.72	0.044

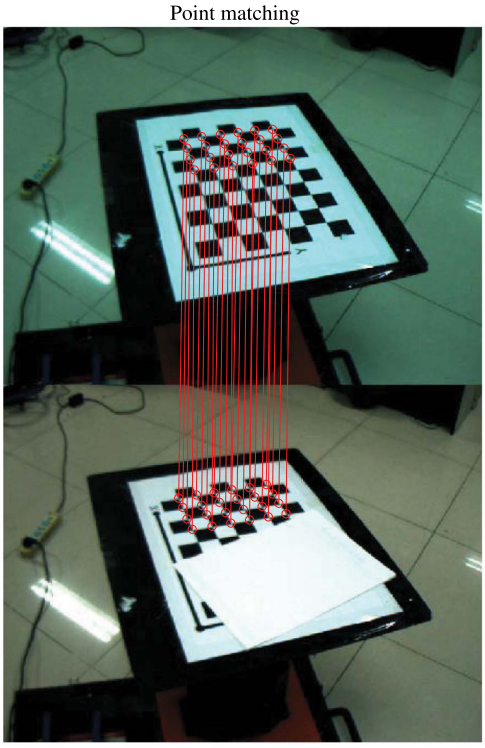

Fig. 13. Point matches in occlusion situations. Even in such a complex environment, our method works well.

proposed method gains a minimum resolution angle of less than 0.09°.

5. *Occlusions*

To demonstrate that the proposed method is suitable in occlusion situations, images with occlusion are tested for Installation 2. The angle errors are shown in Table 3, and the matching results of a certain image are shown in Fig. 13.

6. Conclusion

This paper proposed a practical method to measure single axis rotation angles with conveniently acquirable equipment, such as a camera and a plane target. The superiority of the proposed method over existing angle measurement methods is that it has no special installation and rotation axis information requirements. It is more suitable for testing and correcting angle measurement sensors rather than as a sensor. Thanks to the point detection algorithm of the checkboard, the calibration and measurement are auto completed and pretty robust. The simulations illustrate the robustness of the proposed method with respect to image noises. Then the real image experiments achieve a measurement accuracy of less than 0.1° with a camera and a printed checkboard. Furthermore, the proposed method can be used to measure angles as tiny as 0.09°. Experiments on images with occlusion show that the angle estimation algorithm with point matching works well. Future works will include the extension to measure three axis rotations and an angle measurement toolbox of C++ implementation.

Appendix A

Proof of Theorem 2: According to Theorem 1(i) of the rotation matrix and the translation vector, $[R_{cb}, T_{cb}]$ is obtained directly by

$$T_{cb} = R_z(\theta)T_{ca}, \qquad R_{cb} = R_z(\theta)R_{ca},$$

where

$$R_z(\theta) = \begin{bmatrix} \cos\theta & -\sin\theta & 0 \\ \sin\theta & \cos\theta & 0 \\ 0 & 0 & 1 \end{bmatrix}.$$

By applying Theorem 1(iii), the following equations hold:

$$R_{ba} = R_{ac}R_z(-\theta)R_{ac}^T, T_{ba} = R_{ac}R_z(-\theta)T_{ca} - R_{ac}T_{ca}.$$

Putting $R_{ac} = [r_1, r_2, r_3]$ and $T_{ca} = (t, 0, 0)^T$ into the above equations, one obtains

$$\begin{aligned} R_{ba} &= \cos\theta r_1 r_1^T - \sin\theta r_2 r_1^T \\ &\quad + \sin\theta r_1 r_2^T + \cos\theta r_2 r_2^T + r_3 r_3^T, \\ T_{ba} &= -t[(1-\cos\theta)r_1 + \sin\theta r_2]. \end{aligned}$$

Noting

$$\begin{aligned} r_1 \times R_{ba} &= -\sin\theta r_3 r_1^T + \cos\theta r_3 r_2^T - r_2 r_3^T, \\ r_2 \times R_{ba} &= -\cos\theta r_3 r_1^T - \sin\theta r_3 r_2^T + r_1 r_3^T. \end{aligned}$$

It follows that

$$\begin{aligned} [T_{ba}]_\times R_{ba} &= -t[(1-\cos\theta)r_1 \times R_{ba} + \sin\theta r_2 \times R_{ba}] \\ &= -t(\cos\theta - 1)(r_3 r_2^T + r_2 r_3^T) \\ &\quad + t\sin\theta(r_1 r_3^T - r_3 r_1^T). \end{aligned}$$

On the other hand, r_2 satisfies

$$[r_2]_\times = [r_1 \times r_3]_\times = r_1 r_3^T - r_3 r_1^T.$$

Thus Eq. (8) holds.

References

1. J. A. Bennett, *The Divided Circle: A History of Instruments for Astronomy, Navigation and Surveying* (Phaidon, 1987).
2. G. L. Jung, J. S. Kim, T. H. Lee, J. H. Choi, H. B. Oh, A. H. Kim, G. M. Eom, J. H. Lee, S. C. Chung, J. R. Park, Y. J. Lee, H. J. Park, and J. H. Jun, "Development of an optical fiber sensor

for angular displacement measurements," Biomed. Mater. Eng. **24**, 771–780 (2014).
3. P. Huang, S. Kiyono, and O. Kamada, "Angle measurement based on the internal-reflection effect: a new method," Appl. Opt. **31**, 6047–6055 (1992).
4. L. J. Wuerz and R. C. Quenelle, "Laser interferometer system for metrology and machine tool applications," Precis. Eng. **5**, 111–114 (1983).
5. C. H. Liu, W. Y. Jywe, and S. C. Tzeng, "Simple three-dimensional laser angle sensor for three-dimensional small-angle measurement," Appl. Opt. **43**, 2840–2845 (2004).
6. W. M. Li, J. Jin, X. F. Li, and B. Li, "Method of rotation angle measurement in machine vision based on calibration pattern with spot array," Appl. Opt. **49**, 1001–1006 (2010).
7. J. Jin, L. N. Zhao, and S. L. Xu, "A new high-precision rotation angle measurement method based on monocular vision," J. Opt. Soc. Am. A **31**, 1401–1407 (2014).
8. J. K. Aggarwal and N. Nandhakumar, "On the computation of motion from sequences of images: a review," Proc. IEEE **76**, 917–935 (1988).
9. S. C. Park, H. S. Lee, and S. W. Lee, "Qualitative estimation of camera motion parameters from the linear composition of optical flow," Pattern Recogn. **37**, 767–779 (2004).
10. S. Tan, J. Dale, A. Anderson, and A. Johnston, "Inverse perspective mapping and optic flow: a calibration method and a quantitative analysis," Image Vis. Comput. **24**, 153–165 (2006).
11. M. Marquis-Bolduc, F. Deschênes, and W. Pan, "Combining apparent motion and perspective as visual cues for content-based camera motion indexing," Pattern Recogn. **41**, 445–457 (2008).
12. C. Zhang, Z. Chen, M. Li, and K. Sun, "Direct method for motion estimation and structure reconstruction based on optical flow," Opt. Eng. **51**, 067004 (2012).
13. T. W. Hui and R. Chung, "Determining shape and motion from non-overlapping multi-camera rig: a direct approach using normal flows," Comput. Vis. Image Underst. **117**, 947–964 (2013).
14. B. Caprile and V. Torre, "Using vanishing points for camera calibration," Int. J. Comput. Vis. **4**, 127–139 (1990).
15. J. Weng, P. Cohen, and M. Herniou, "Camera calibration with distortion models and accuracy evaluation," IEEE Trans. Pattern Anal. Mach. Intell. **14**, 965–980 (1992).
16. Z. Y. Zhang, "A flexible new technique for camera calibration," IEEE Trans. Pattern Anal. Mach. Intell. **22**, 1330–1334 (2000).
17. J. Y. Bouguet, "Camera Calibration Toolbox for MATLAB," (2004),. http://www.vision.caltech.edu/bouguetj/calib_doc/.
18. W. Niem and R. Buschmann, "Automatic modelling of 3D natural objects from multiple views," in *Image Processing for Broadcast and Video Production* (Springer, 1995), pp. 181–193.
19. V. Fremont and R. Chellali, "Turntable-based 3D object reconstruction," in *IEEE Conference on Cybernetics and Intelligent Systems*(IEEE, 2004), pp. 1277–1282.
20. H. S. Sawheny, J. Oliensis, and A. R. Hanson, "Image description and 3-D reconstruction from image trajectories of rotational motion," IEEE Trans. Pattern Anal. Mach. Intell. **15**, 885–898 (1993).
21. A. W. Fitzgibbon, G. Cross, and A. Zisserman, "Automatic 3D model construction for turn-table sequences," in *3D Structure from Multiple Images of Large-Scale Environments* (Springer, 1998), pp. 155–170.
22. A. Geiger, F. Moosmann, O. Car, and B. Schuster, "Automatic camera and range sensor calibration using a single shot," in *IEEE International Conference on Robotics and Automation* (IEEE, 2012), pp. 3936–3943.
23. P. Neumann, "Representation of orientations of symmetrical objects by Rodrigues vectors," Texture Microstruct. **14**, 53–58 (1991).
24. B. Triggs, P. F. McLauchlan, R. I. Hartley, and A. W. Fitzgibbon, "Bundle adjustment—a modern synthesis," in *Vision Algorithms: Theory and Practice* (Springer, 2000), pp. 298–372.
25. J. J. Moré, "The Levenberg–Marquardt algorithm: implementation and theory," in *Numerical Analysis* (Springer, 1978), pp. 105–116.
26. http://www.reinovo.com/html/index.asp.
27. http://quanquan.buaa.edu.cn/Anglemeasurementtoolbox.html.